Single vortex states in a confined Bose-Einstein condensate

S. Komineas and N. R. Cooper
Theory of Condensed Matter Group, Cavendish Laboratory, Madingley Road, Cambridge CB3 0HE, United Kingdom

N. Papanicolaou
Department of Physics, University of Crete, and Research Center of Crete, Heraklion, Greece
(Received 25 August 2005; published 21 November 2005)

It has been demonstrated experimentally that non-axisymmetric vortices precess around the center of a Bose-Einstein condensate. Two types of single vortex states have been observed, usually referred to as the S vortex and the U vortex. We study theoretically the single vortex excitations in spherical and elongated condensates as a function of the interaction strength. We solve numerically the Gross-Pitaevskii equation and calculate the angular momentum as a function of precession frequency. The existence of two types of vortices means that we have two different precession frequencies for each angular momentum value. As the interaction strength increases the vortex lines bend and the precession frequencies shift to lower values. We establish that for given angular momentum the S vortex has higher energy than the U vortex in a rotating elongated condensate. We show that the S vortex is related to the solitonic vortex, which is a nonlinear excitation in the nonrotating system. For small interaction strengths the S vortex is related to the dark soliton. In the dilute limit a lowest Landau level calculation provides an analytic description of these vortex modes in terms of the harmonic oscillator states.

DOI: 10.1103/PhysRevA.72.053624 PACS number(s): 03.75.Lm, 03.75.Kk

I. INTRODUCTION

Quantized vortices in superfluids have been the subject of an important research area since their theoretical prediction in the context of liquid helium [1]. In the last years there has been intense experimental and theoretical study on the creation and dynamics of single vortices as well as vortex lattices in ultracold atomic Bose-Einstein condensates (BECs) [2,3]. These systems offer the possibility for direct observation of vortex lines and of their dynamics. They are thus excellent systems for a comprehensive theoretical study of vortex lines in three dimensions.

In an experiment performed in a spherical trap [4] single vortices were produced by a technique that induces a 2π phase winding using a rotating laser beam. The vortices were located off the trap center, and they were seen to precess robustly around it at an almost constant angular velocity. Surprisingly the precession frequency was found to be almost independent of the displacement of the vortex from the trap center.

In another important experiment it was established that the vortex lines in the finite trap geometry can have nontrivial shapes [2]. It was observed that a single vortex line may have an S shape or a U shape. The length and precise shape of the vortex can vary and this is directly related to the angular momentum it carries. Theoretical work in high-density very elongated condensates similar to those of Ref. [2] showed that the U-shaped vortex can be the ground state of the rotating system [5,6]. Some differences between the S and the U-vortex were reported in Ref. [7].

In this paper, we establish that an axisymmetric BEC generically supports both S- and U-shaped vortices. We study these single vortices as precessing stationary states within the nonlinear Gross-Pitaevskii theory for a range of interaction strengths. Their frequency of precession around the trap center depends critically on the features of the vortex line. Precession frequencies for U vortices depend only weakly on their angular momentum and fall in a relatively narrow frequency range that depends on the interaction strength. S vortices have higher energy and their precession frequencies depend strongly on their angular momentum. The nonrotating member of this family is a non-axisymmetric vortex solution of the nonlinear theory. This has been called a *solitonic vortex*; it breaks spontaneously the symmetry in an axially symmetric potential and pierces through the trap in a direction perpendicular to the symmetry axis [8,9].

In the dilute limit the low-energy states can be described within a lowest Landau level (LLL) ansatz [10]. Motivated by the fact that experiments are usually performed in elongated condensates we generalize the LLL ansatz to include longitudinal modes. Both types of single vortex states can then be described within this formalism and some simple analytic expressions capture the main features of the vortex modes. Low-density condensates close to the LLL regime have been created recently by fast rotation, where a vortex lattice was formed [11].

The outline of the paper is as follows. In Sec. II we formulate the problem and find numerically two types of single vortex solutions of the Gross-Pitaevskii equation. We apply our method for a spherical trap as in Ref. [4] as well as for elongated condensates. In Sec. III we formulate the problem in the LLL augmented to include the longitudinal modes and we study the S and U vortices within this formalism. Finally, Sec. IV contains a summary and our concluding remarks.

II. PRECESSING VORTICES

Motivated by the experiment [4] where off-center vortices precess at an almost constant angular velocity around the

center of the condensate, we look here for vortices that are stationary states in a frame rotating at a constant frequency. In this paper we suppose that the energy of a BEC is given by the Gross-Pitaevskii theory. We consider an axially symmetric harmonic potential with frequencies $\omega_\perp$ in the transverse direction and $\omega_\parallel$ in the longitudinal direction and implement rationalized units by the substitutions

$$x \to a_\perp x, \quad y \to a_\perp y, \quad z \to a_\parallel z, \quad \Psi \to \frac{N^{1/2}}{a_\perp a_\parallel^{1/2}} \Psi, \quad (1)$$

where Ψ is the condensate wave function, N is the number of atoms in the condensate, and $a_{\perp,\parallel} = \sqrt{\hbar/m\omega_{\perp,\parallel}}$ are the oscillator lengths in the transverse and longitudinal directions. The wave function normalization condition reads as

$$\int |\Psi|^2 \, dV = 1. \quad (2)$$

The energy functional per particle in units of $\hbar\omega_\perp$ has the form

$$E = \frac{1}{2} \int \left[|\nabla_\perp \Psi|^2 + \rho^2 |\Psi|^2 + \beta \left(\left| \frac{\partial \Psi}{\partial z} \right|^2 + z^2 |\Psi|^2 \right) + 4\pi \frac{N a_s}{a_\parallel} |\Psi|^4 \right] dV, \quad (3)$$

where ρ, z, and ϕ are cylindrical coordinates, $\nabla_\perp$ is the gradient on the transverse plane, a_s is the scattering length, and the parameter

$$\beta \equiv \frac{\omega_\parallel}{\omega_\perp} \quad (4)$$

is the ratio of the two frequencies. The value $\beta = 1$ corresponds to a spherical trap. The quartic term gives the strength of the interactions and we introduce for later convenience the parameter

$$\delta \equiv \frac{1}{2\sqrt{2\pi}} \frac{N a_s}{a_\parallel}, \quad (5)$$

which is a dimensionless measure of the interaction strength relative to the transverse trapping energy $\hbar\omega_\perp$.

Stationary states that precess at a constant angular frequency ω are extrema of the energy in the rotating frame:

$$E_{\rm rot} = E - \omega \ell \, , \quad (6)$$

where ℓ is the angular momentum per particle along the symmetry axis, in units of $\hbar$:

$$\ell = \frac{1}{i} \int \Psi^* \frac{\partial \Psi}{\partial \phi} \, dV. \quad (7)$$

The asterisk denotes complex conjugation, and the frequency ω is measured in units of $\omega_\perp$.

Extremizing numerically the energy functional (6) is often not practically convenient because some of the interesting solutions may not correspond to its minima. Therefore, we define the Lyapunov functional

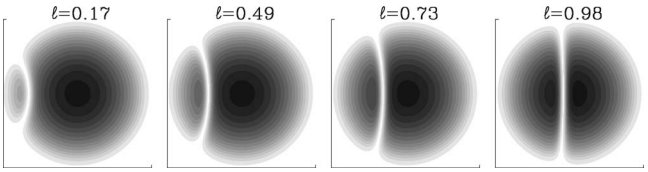

FIG. 1. The particle density $|\Psi|^2$ for vortex solutions of the Gross-Pitaevskii model in a spherical trap ($\beta=1$) at $\delta=85$. The parameters correspond to the conditions of the experiment [4]. We show the plane containing the vortex line and the z axis along which the angular momentum ℓ is measured. The images correspond to four representative values of $\ell=0.17, 0.49, 0.73, 0.98$ with precession frequencies $\omega=0.268, 0.221, 0.205, 0.196$, respectively, in units of $\omega_\perp$. The size of the frames shown is 12×12 in units of $a_\perp$. White color corresponds to no particles and black color to maximum particle density.

$$E'_{\rm rot} = E + \frac{a_1}{2}(\ell - b_1)^2, \quad (8)$$

where we have introduced the constants a_1, b_1. An extremum of $E'_{\rm rot}$ corresponds to an extremum of $E_{\rm rot}$ with $\omega = a_1(b_1 - \ell)$. We find the minima of $E'_{\rm rot}$ by using a variant of a numerical norm-preserving relaxation algorithm [12] which, in effect, capitalizes on a virial relation [13] in order to converge to a wave function of unit norm. The method is applied on a three-dimensional grid in Cartesian coordinates. The advantage of using $E'_{\rm rot}$ is that we can find stationary points that are not necessarily minima of $E_{\rm rot}$. The constants a_1, b_1 should be chosen so as to ensure convergence to the desired value of the angular momentum, say ℓ_0. This usually amounts to choosing b_1 close to ℓ_0, while a_1 should be positive and large enough so that the stationary point at ℓ_0 be a minimum. Once the solutions for a range of angular momenta are known the frequency is given by $\omega = dE/d\ell$.

We first apply the method for parameters similar to those in Ref. [4]: $\beta=1$ and $\delta=85$. Since the trap is spherical any arbitrary axis in space can be chosen as the z axis along which ℓ is measured. We find vortex states for the range of angular momenta $0 < \ell \leqslant 1$ and we present images of the particle density for some representative ones in Fig. 1. The condensate is at the nonrotating spherically symmetric ground state for $\ell=0$. For $\ell>0$ a vortex line enters the condensate. As ℓ is increased the vortex line is closer to the center and it is curved for $\ell<1$; it becomes the axially symmetric vortex at the center of the condensate for $\ell=1$. Following Refs. [2,7] we call the vortex mode in Fig. 1 the *U vortex*.

The angular momentum ℓ as a function of the precession frequency ω of the vortex around the z axis is shown in Fig. 2. We find that single vortex states with $0<\ell<1$ have frequencies in the range $0.195<\omega<0.35$. However, except for very low values of ℓ, the branch has frequencies in a narrow frequency range, say, $\omega \approx 0.195$ to 0.25. In physical units the frequency f defined from $\omega = 2\pi f$ takes values in the range 1.52 Hz $< f <$ 1.95 Hz (e.g., $f=1.72$ Hz for $\ell=0.5$); which is in agreement with the value 1.8 Hz measured in [4]. In Ref. [14] the precession frequency of the vortex is explained in terms of an anomalous mode of the Bogoliubov spectrum

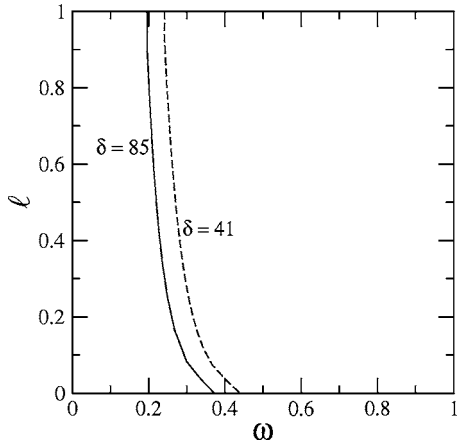

FIG. 2. Angular momentum per particle ℓ (in units of $\hbar$) as a function of the precession frequency ω (in units of $\omega_\perp$) for $\beta=1$, $\delta=85$ (solid line), which corresponds to Fig. 1 (and to experiment [4]). We have a U-vortex branch with precession frequencies $0.195<\omega<0.35$. We include the corresponding line (dashed) for a smaller interaction strength $\delta=41$ for comparison.

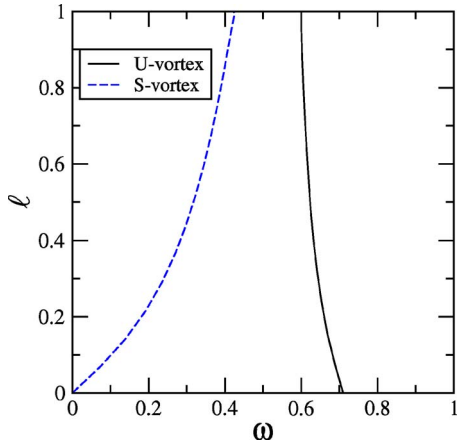

FIG. 3. (Color online) Angular momentum per particle ℓ (in units of $\hbar$) as a function of the precession frequency ω (in units of $\omega_\perp$) for vortices in an axially symmetric elongated trap with $\beta=1/2$, $\delta=2$. The solid line shows the U-vortex branch. The dashed line is the S-vortex branch which contains the solitonic vortex for $\ell=0$ (at $\omega=0$). Both modes give the axially symmetric vortex for $\ell=1$, but this is obtained at different limiting frequencies: $\omega=0.60$ for the U vortex and $\omega=0.44$ for the S vortex.

and it is related to its stability. The frequencies 1.58 Hz given in the above reference should be compared with the limiting frequency (1.52 Hz) obtained in our calculation. A somewhat counterintuitive feature of the results presented in Fig. 2 is that the precession frequency decreases as the angular momentum increases, which means that vortices closer to the axis precess slower. This point is discussed further at the end of this section in connection with stability.

Further in this section we expand our calculations to axially symmetric elongated traps. This is an important direction since the majority of experiments involving vortices have been performed in elongated condensates. Previous theoretical work on few-vortex solutions has focused on very dense elongated condensates which are practically in the Thomas-Fermi regime [5–7] and satisfy the condition $\delta \gg 1, \beta$. In this section we shall focus on the regime $\delta \sim 1$.

Here we present a calculation for $\beta=1/2$ and $\delta=2$. Using Na atoms and trapping frequencies $\omega_\perp=2\pi\times 7.8$ Hz, $\omega_\parallel=\omega_\perp/2$, these values are obtained for $N=27\,000$ atoms ($N=6700$ for Rb). In Fig. 3 we show by a solid line the angular momentum for the U vortex as a function of the precession frequency. The angular momentum is a decreasing function of ω, and the precession frequency range over which the U vortex exists is narrow and it is located at much higher frequencies compared to Fig. 2. In Fig. 4 we present images of the U vortices for various values of the angular momentum. Vortices are off center and slightly curved. The axially symmetric vortex is obtained as the limit for a frequency $\omega_U=0.60$.

References [8,9,15] study a solution of the Gross-Pitaevskii equation that has been called the *solitonic vortex*. This appears to be different than all the vortices discussed in this section so far. The solitonic vortex is an excited state in an elongated nonrotating condensate that pierces through the trap in a direction perpendicular to the symmetry axis and therefore it has angular momentum $\ell=0$ (along the symmetry axis). An example is shown in the first entry of Fig. 5. The solitonic vortex exists for sufficiently high interaction strengths and it bifurcates from the dark soliton solution.

We notice that the solitonic vortex breaks spontaneously the axial symmetry and if we assume a finite precession frequency ω, it may acquire a nonvanishing angular momentum $\ell=\ell(\omega)$. In order to explore this possibility we use the solitonic vortex solution as an initial guess in our numerical algorithm and choose appropriate values for the constants in Eq. (6). Representative results for vortex solutions with $0 \leqslant \ell \leqslant 1$ are shown in Fig. 5, for an elongated condensate ($\beta=1/2$) and for an interaction strength constant $\delta=2$. The first entry, for $\ell=0$, is the solitonic vortex and the next entries show almost straight vortex lines that are tilted with respect to the z axis. As the frequency increases the vortex line progressively aligns with the symmetry axis while its angular momentum increases. The dependence of ℓ on ω is shown by a dashed line in Fig. 3. This mode, which may be called the *S-vortex* following Ref. [7], gives the axially sym-

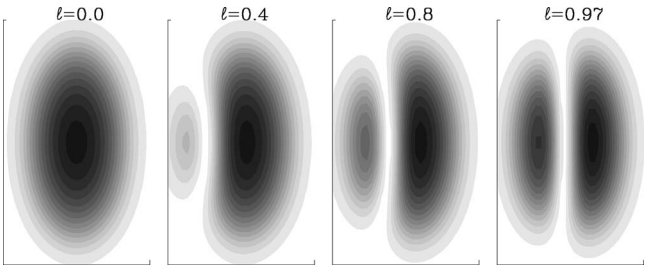

FIG. 4. The particle density $|\Psi|^2$ for the U vortex corresponding to the solid line in Fig. 3 ($\beta=1/2, \delta=2$) for four values of the angular momentum ℓ. Here we show the plane containing the symmetry axis and the vortex line. At $\ell=0$ we have the nonrotating ground state and for $\ell=1$ we obtain the axially symmetric vortex. For $0<\ell<1$ the vortex lines are slightly curved. The size of the frames shown is 6×10 (in units of $a_\perp$).

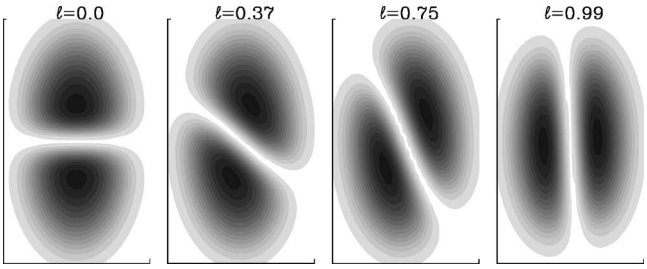

FIG. 5. The particle density $|\Psi|^2$ for the S vortex corresponding to the dashed line in Fig. 3 ($\beta=1/2, \delta=2$) for four values of the angular momentum ℓ. We show here the plane containing the symmetry axis and the vortex line. At $\ell=0$ we have the *solitonic vortex* and for $\ell=1$ we obtain the axially symmetric vortex. For $0<\ell<1$ the vortex lines are slightly curved. The size of the frames shown is 6×10 (in units of $a_\perp$).

metric vortex ($\ell=1$) at a limiting frequency $\omega_S=0.44$ [this value should be compared with Eq. (13) in Sec. III.] Thus the S and the U vortex are two different types of single vortex states in elongated condensates.

The picture summarized in Figs. 3, 4, and 5 is apparently robust for large interaction strengths. In particular, in the experiments in Ref. [2] and in Refs. [5–7], S and U vortices are found in condensates that are practically in the Thomas-Fermi regime ($\delta\gg1, \beta$). Unlike in the present case, all vortices were found to be distinctly curved. Also, in Ref. [7] the limiting ($\ell=1$) frequencies for the axially symmetric vortex appear to coincide for both the S vortex and the U vortex. These differences should be attributed to the Thomas-Fermi nature of the condensates studied in the above references.

In order to complete the study of S vortices, we note that the qualitative picture should be modified for low interaction strengths. This is because the solitonic vortex is a solution of the nonlinear theory that exists only above a certain value of the interaction strength, $\delta>\delta_0$, which depends on β [9,15]. In order to explore the regime $\delta<\delta_0$ we choose $\delta=0.28$ in the elongated trap with $\beta=1/2$. Figure 6 shows the angular momentum of the vortex modes as a function of the precession frequency. A substantial modification for the S vortex is that now $\ell\to0$ for a finite limiting frequency $\omega=0.26$. For $\omega\leqslant0.26$ we obtain an axially symmetric wave function with a node on the $z=0$ plane, which, in the context of the present nonlinear theory, is called a *dark soliton* by comparison to the dark soliton of the nonlinear Schrödinger equation. Summarizing, the picture in Fig. 6 could also be described as the following: a dark soliton that may initially be created in a trap would not respond to rotations of the system until we exceed a limiting frequency 0.26. For $\omega>0.26$ it could turn into an S vortex that would become an axially symmetric one for $\omega>0.49$ [these frequencies should be compared with Eq. (16) in Sec. III when setting $\ell=0$ and $\ell=1$, respectively.] Finally, we note that the particle density plots for the S vortices are qualitatively similar to those for higher interaction strengths presented above (as in Fig. 5), except, of course, for the $\ell=0$ case.

The U-vortex branch is qualitatively similar to its counterpart for $\delta=2$ but its frequency range is shifted closer to the transverse trapping frequency ($\omega_\perp$) while it becomes narrower as δ decreases.

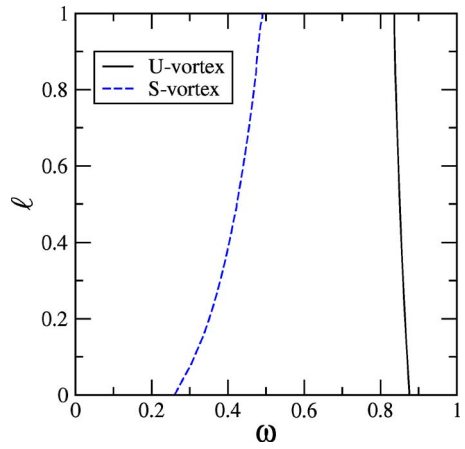

FIG. 6. (Color online) Angular momentum per particle ℓ (in units of $\hbar$) as a function of the precession frequency ω (in units of $\omega_\perp$) for vortices in an axially symmetric elongated trap with $\beta=1/2$, $\delta=0.28$. The solid line shows the U-vortex branch. The dashed line is the S vortex for which the $\ell=0$ state (for $\omega\leqslant0.26$) is a dark soliton. Both modes become the axially symmetric vortex at the limit $\ell\to1$, but this is obtained at different frequencies.

In Ref. [13] a series of virial relations are derived that should be satisfied by any vortex solution. We have checked that the solutions presented here have, in particular, the counterintuitive property that the moments of the particle density vanish: $\int x|\Psi|^2\,dV=\int y|\Psi|^2\,dV=\int z|\Psi|^2\,dV=0$. This is trivially satisfied by the S vortex due to its symmetry along the z axis, but it is a nontrivial result for the U vortex.

We comment briefly on the relation of the vortex modes presented here to vortices in helium II. In Ref. [16] an equation is derived for the dynamics of a vortex line in a rotating bucket containing the superfluid and it is found that there are vortex lines precessing on an unstable orbit around the bucket center at some distance r, which is an increasing function of the precession frequency. Since the angular momentum of the vortex is a decreasing function of r (as discussed in Ref. [17]), we conclude that the angular momentum is a decreasing function of the precession frequency, that is the situation is analogous to that for the U vortex in Figs. 2, 3, and 6.

We finally turn to the delicate issue of stability of the calculated vortex states. According to Ref [10], "mechanical stability" requires that the energy be a convex function of angular momentum: $d\omega/d\ell=d^2E/d\ell^2>0$. However, this is a condition for stability of the solution in the rotating frame under variations that change the angular momentum. In experiments in which the trap is axially symmetric (i.e., when the system is no longer being stirred), the angular momentum is conserved and this condition is irrelevant for the stability of the modes: what is relevant is that the mode should be *dynamically stable* against decay into other modes that have the same angular momentum. As is evident from Fig. 2, the precessing U vortex has $d\omega/d\ell<0$, so it does not satisfy the criterion of the mechanical stability of Ref. [10]. However, the U vortex must be dynamically stable since it is the lowest-energy configuration for given angular momentum $0<\ell<1$, as we know from the calculations in the present

section. Indeed the U vortex has been seen in experiments [4] in which angular momentum is conserved.

It is also interesting to comment on the issue of overall *thermodynamic* stability of the rotating system. In the rotating frame, a single axially symmetric ($\ell=1$) vortex is the lowest-energy state if $\omega > E_V - E_0$ where E_V and E_0 are the vortex and the ground state energies in the laboratory frame [1]. Now, taking into account that $\omega = dE/d\ell$, we may write

$$E_V - E_0 = \int_0^1 \omega(\ell) d\,\ell\ . \tag{9}$$

Applying this relation for the U vortex calculated for a spherical trap with $\delta=85$ (see Fig. 2) we find $E_V - E_0 = 0.23$ or, in physical units, 1.8 Hz, which lies in the range of precession frequencies for the U vortex.

III. DILUTE CONDENSATES

We now turn to discuss more specifically dilute condensates that offer the possibility to study vortex modes in the limit of a small interaction strength where the energy levels of the system are close to those of the harmonic oscillator. This analysis will provide an analytic description of the features of the S and U vortices. In Ref. [10] the energy $E_{\rm rot}$ of a rotating system is minimized in the case of the very dilute limit in the sense that the nonlinear term in Eq. (3) is much smaller than the other energy scales, namely $\hbar\omega_\perp, \hbar\omega_\parallel$, or

$$\delta \ll 1, \beta. \tag{10}$$

The problem is then reduced to the lowest Landau level (LLL) on the transverse plane ($\delta \ll 1$) while the wave function in the longitudinal direction z is the Gaussian ground state of the 1D harmonic oscillator. We refer to this as the 2D LLL regime. An analytic solution for vortices with angular momentum in the range $0 < \ell \leqslant 1$ is given in Ref. [18]. The minimization of $E_{\rm rot}$ gives the Gaussian nonrotating ground state as the global minimum for $\omega < \omega_U \equiv 1-\delta$. For $\omega > \omega_U$ the axially symmetric vortex becomes the global minimum of the functional (6). Exactly at $\omega = \omega_U$ there is a set of states with $0 < \ell < 1$ that are off-center vortices. These are denoted by a solid line in Fig. 7 that shows the angular momentum as a function of the precession frequency. For higher values of ω (but still lower than the transverse frequency of the potential), many-vortex states and vortex lattices become the absolute minimum [10,18]. All vortex lines are parallel to the symmetry axis of the trap since this is a 2D calculation. For larger values of δ these evolve in the curved vortex lines as, e.g., in Fig. 1 and thus they correspond to the U-vortex mode discussed in the previous section.

In elongated traps excited states of the rotating condensate can be found without mixing higher Landau levels. This is an interesting issue also because most experiments involving vortices, and in particular those in which the shapes of individual vortex lines were studied, were performed in very elongated traps, that is, at $\beta \ll 1$ [2]. We first consider the case of a noninteracting gas, i.e., $\delta=0$, whose first excited state has a node in the z direction:

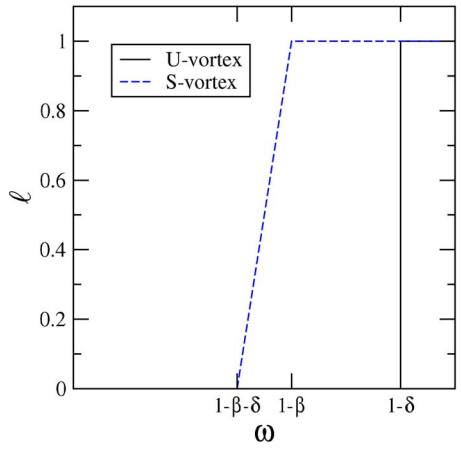

FIG. 7. (Color online) Angular momentum per particle ℓ (in units of $\hbar$) as a function of the precession frequency ω (in units of $\omega_\perp$) for $\delta \ll 1, \beta, 1-\beta$ for single vortex states. The solid line is the result of Ref. [10]. The dashed line is a plot of Eq. (16). The horizontal axis is not to scale. The wave function at $\ell=0$ for the dashed line ($\omega \leqslant 1-\beta-\delta$) is Ψ_1, while for the solid line ($\omega \leqslant 1-\delta$) it is the Gaussian. The $\ell=1$ state is Ψ_2 for both cases.

$$\Psi_1 = \frac{\sqrt{2}}{\pi^{3/4}} z e^{-(\rho^2+z^2)/2}, \tag{11}$$

its energy is $E_1=\beta$, and has vanishing angular momentum. Here, we have substrated the ground state energy of the harmonic oscillator $1+\beta/2$, a convention that will be adopted from now on. We note that for increasing δ the wave function Ψ_1 evolves to the dark soliton in the framework of the nonlinear Gross-Pitaevskii model. A further excited state is of the vortex type

$$\Psi_2 = \frac{1}{\pi^{3/4}} \rho e^{i\phi} e^{-(\rho^2+z^2)/2}, \tag{12}$$

and it has energy $E_2=1$ and angular momentum $\ell=1$. It is thus obvious that for the frequency,

$$\omega_S = 1-\beta, \tag{13}$$

the two states (11) and (12) have the same energy $E_{\rm rot}$ in the rotating frame. For $\omega < \omega_S$ we have Ψ_1 as the first excited state while Ψ_2 becomes the first excited state for $\omega > \omega_S$.

The simple picture is modified in the presence of a weak interaction term, that is, for δ small but finite. For $\delta \ll \beta, 1-\beta$ we make the ansatz

$$\Psi = c_1 \Psi_1 + c_2 \Psi_2, \tag{14}$$

where the coefficients c_1, c_2 are constrained by $|c_1|^2 + |c_2|^2 = 1$ and $|c_2|^2 = \ell$. Substituting Ψ in Eq. (3), we find the energy of the first excited state as a function of the angular momentum ℓ:

$$E(\ell) = \frac{\delta}{2}\ell^2 + (1-\beta-\delta)\,\ell\ + \beta + \frac{3\delta}{2}. \tag{15}$$

Now, $E_{\rm rot}(\ell)$ has a minimum for any ℓ in the range $0 < \ell < 1$ and a frequency $\omega = dE/d\ell$ or

$$\omega = 1 - \beta - \delta(1 - \ell), \tag{16}$$

as depicted by the dashed line in Fig. 7. For $\omega \leqslant 1-\beta-\delta$ the wave function is $\Psi=\Psi_1$ ($\ell=0$) while for $\omega \geqslant 1-\beta$ we have $\Psi=\Psi_2$ ($\ell=1$).

The vortex line represented by the ansatz (14) is found by setting

$$\Psi = 0 \Rightarrow \sqrt{2}c_1 z + c_2(x+iy) = 0 \Rightarrow y = 0, \sqrt{2}c_1 z + c_2 x = 0, \tag{17}$$

where, for simplicity, we may consider c_1, c_2 real. For frequencies in the range $1-\beta-\delta<\omega<1-\beta$ we have $c_1, c_2 \neq 0$, and thus Eq. (17) gives a straight vortex line that is tilted with respect to the symmetry axis z. Summarizing, the first excited state (14) has a wave function with a nodal plane perpendicular to the z axis for low frequencies that turns to a tilted vortex for $1-\beta-\delta<\omega<1-\beta$. This gradually aligns with the symmetry axis as the frequency increases. It becomes the axially symmetric vortex above the limiting frequency $\omega \geqslant \omega_S = 1-\beta$. This is the weak interaction limit of the S vortex discussed in the previous section.

Both the S vortex and the U vortex become the axially symmetric vortex for a sufficiently high ω. However, the corresponding limiting frequencies for the two types of vortices do not coincide. In fact, there is no sense of precession in an axially symmetric vortex and the limiting frequency may be absorbed into an effective chemical potential $\bar{\mu}=\mu+\omega$ while the wave function reduces to a quasistatic configuration with chemical potential $\bar{\mu}$.

We are able to take our calculation one step further if we assume a very elongated trap, i.e., $\beta \ll 1$, and an interaction strength comparable to the latter energy scale:

$$\delta \ll 1 \quad \text{and} \quad \delta \sim \beta. \tag{18}$$

In this case it is useful to extend the LLL calculation to three dimensions by including higher axial oscillator states. We use the wave function ansatz

$$\Psi(\rho, z, \phi) = \sum c_{mn} \chi_m(\rho, \phi) \xi_n(z), \tag{19}$$

where c_{mn} are complex constants,

$$\chi_m(\rho, \phi) = \left(\frac{1}{\pi m!}\right)^{1/2} e^{im\phi} \rho^m e^{-\rho^2/2} \tag{20}$$

are eigenstates of the 2D harmonic oscillator, and

$$\xi_n(z) = \left(\frac{2^n}{(2n-1)!!}\right)^{1/2} \frac{1}{\pi^{1/4}} z^n e^{-z^2/2} \tag{21}$$

form a basis for the expansion of the wave function in the axial direction. We aim to find the vortex states for a fixed angular momentum within the present ansatz. An efficient way to do this is by minimizing the Lyapunov functional,

$$E''_{\text{rot}} = E + \frac{a_1}{2}(\ell - b_1)^2 + \frac{a_2}{2}(\nu - b_2)^2, \tag{22}$$

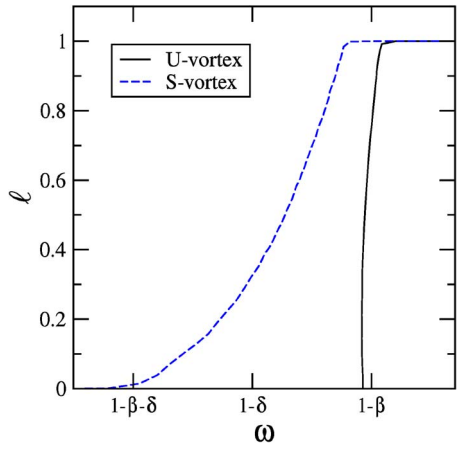

FIG. 8. (Color online) Angular momentum per particle ℓ (in units of $\hbar$) as a function of the precession frequency ω (in units of $\omega_\perp$) for the S vortex (dashed line) and U vortex (solid line) within the 3D LLL calculation for $\delta/\beta=2$. Here, $d\ell/d\omega>0$ (except for small values of ℓ) unlike in Fig. 7.

where ℓ is the angular momentum functional of Eq. (7) and $\nu \equiv \int |\Psi|^2 \, dV$. The constants a_1, a_2, b_1, b_2 are chosen so as to obtain a solution for the desired number of particles and angular momentum. We substitute the wave function (19) in Eq. (22) and minimize E''_{rot} with respect to c_{mn} by a conjugate gradient method. Computer limitations allow for modes typically up to $m=4$ and $n=14$.

When the interaction term is small, i.e., $\delta \ll \beta$ the algorithm converges to the two single-vortex solutions that were discussed in Fig. 7. Specifically, for the U vortex we have that all c_{mn} with $n \neq 0$ vanish. For the S vortex we have that only c_{01}, c_{10} are nonzero. When δ becomes comparable or greater than β several c_{mn} are nonzero and their values decrease with respect to both indices. For the S vortex we find that all c_{mn} with $m+n$ even vanish, and this is consistent with the symmetry of an S-shaped vortex. For the U vortex we find that for all n odd $c_{mn}=0$, which is consistent with the symmetry of a U-shaped vortex.

Figure 8 shows the angular momentum of the two vortices as a function of the precession frequency for parameter values $\delta/\beta=2$. The most dramatic effect is seen in the U vortex where $d\ell/d\omega$ is now positive, except for small values of ℓ. This means that the abrupt transition from the $\ell=0$ to the $\ell=1$ state depicted in Fig. 7 is smoothed out and the angular momentum of the U vortex is now a smooth function of the frequency ω, although the range of frequencies corresponding to $0<\ell<1$ is narrow. The vortices in the latter range are located off center while the contribution of modes with $n>0$ in the wave function (19) means that vortex lines are curved. The S-vortex lines are also curved and the slope of the branch (the dashed line in Fig. 8) is not constant, unlike in Fig. 7.

A concise presentation of the main features of the two vortex modes can be given by the graph of the energy as a function of the angular momentum shown in Fig. 9. The energy of the U-vortex mode for $\ell=0$ is the energy of the nonrotating ground state. The corresponding value for the S vortex is the energy of the wave function Ψ_1. The S vortex

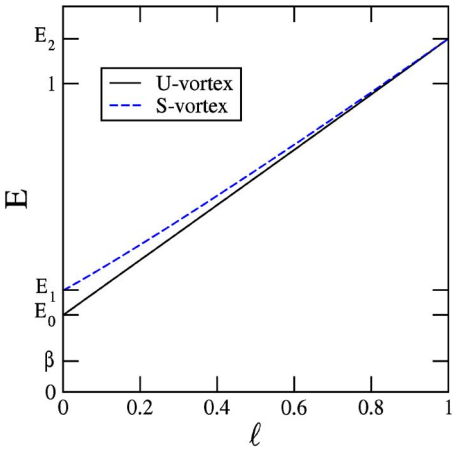

FIG. 9. (Color online) The energy per particle E (in units of $\hbar\omega_\perp$) of Eq. (3) as a function of the angular momentum per particle ℓ (in units of $\hbar$) for the S vortex (dashed line) and the U vortex (solid line) of Fig. 8, where $\delta/\beta=2$. The energies of the nonrotating ground state, and of the wave functions Ψ_1 and Ψ_2, are E_0, E_1, and E_2 correspondingly. (In the noninteracting system the corresponding energies are 0, β, and 1, having subtracted the ground state energy of the harmonic oscillator $1+\beta/2$.)

has higher energy than the U vortex, but both curves converge to the same value for $\ell=1$, which is the energy of the axially symmetric vortex Ψ_2.

IV. CONCLUSIONS

We have analyzed the two single vortex modes, the S vortex and the U vortex, which are stationary states of the Gross-Pitaevskii model precessing at a constant frequency ω in a BEC confined in an axially symmetric harmonic potential. Vortices for the whole range of angular momenta $0 \leqslant \ell \leqslant 1$ have been studied. The precession frequency range is distinctly different for the two modes. The U vortices fall within a relatively narrow frequency range. For those U vortices studied in Sec. II, we find that the precession frequency is a decreasing function of the angular momentum. The S vortex is an excited state in elongated condensates. Their frequency range extends down to zero (for sufficiently high interaction strengths) and the nonrotating member of the family is the so-called solitonic vortex, which is a solution of the nonlinear Gross-Pitaevskii model [8,9]. Both the U vortex and the S vortex have been directly seen in the experiment [2,4]. Perhaps the S vortex is also related to shape deformations of vortex lines observed in the form on Kelvin modes [19,20].

A complete analysis for vortex solutions could be carried out for a dilute condensate within a 3D lowest Landau level calculation that includes the axial oscillator states. We have given a derivation for the S vortex that is complementary to the LLL calculation for the U vortex [10]. Including the axial oscillator states causes the transition from a nonrotating ground state to an axially symmetric vortex to occur smoothly as the rotation frequency increases: vortices with an angular momentum ℓ of less than unity are thermodynamically stable.

Both the S vortex and the U vortex become axially symmetric in the limit $\ell \to 1$, but this occurs at different frequencies in the two cases. This seems to be in disagreement with the results reported in Ref. [7], however, one should note that in the latter reference very elongated and very dense condensates are studied. Although the results are related, an extrapolation of our results to the Thomas-Fermi regime, and thus a direct comparison to Ref. [7], does not appear straightforward. We further find that, for weak interactions, an S vortex line is only slightly bent, in contrast to the original observations in Ref. [2]. In fact, both vortex modes in the dilute limit presented in Fig. 7 represent straight vortex lines. However, as the density increases vortex lines tend to bend (as, e.g., in Figs. 4 and 5). Thus, the difference between the present results and the observations is clearly due to the difference in the density of the condensates.

ACKNOWLEDGMENTS

S.K. is grateful to the ENS group for hospitality and for discussions. S.K. and N.R.C are grateful to the Kavli Institute of Theoretical Physics in Santa Barbara for hospitality and acknowledge discussions during the "Quantum gases" program from which this work has benefited. This work was supported by EPSRC Grants No. GR/R96026/01 (SK) and No. GR/S61263/01 (NRC).

[1] R. J. Donnelly, *Quantized vortices in Helium* II (Cambridge University Press, Cambridge, 1991).
[2] P. Rosenbusch, V. Bretin, and J. Dalibard, Phys. Rev. Lett. **89**, 200403 (2002).
[3] J. R. Abo-Shaeer, C. Raman, J. M. Vogels, and W. Ketterle, Science **292**, 476 (2001).
[4] B. P. Anderson, P. C. Haljan, C. E. Wieman, and E. A. Cornell, Phys. Rev. Lett. **85**, 2857 (2000).
[5] J. J. Garcia-Ripoll and V. M. Perez-Garcia, Phys. Rev. A **64**, 053611 (2001).
[6] M. Modugno, L. Pricoupenko, and Y. Castin, Eur. Phys. J. D **22**, 235 (2003).
[7] A. Aftalion and I. Danaila, Phys. Rev. A **68**, 023603 (2003).
[8] J. Brand and W. P. Reinhardt, J. Phys. B **34**, L113 (2001).
[9] S. Komineas and N. Papanicolaou, Phys. Rev. A **68**, 043617 (2003).
[10] D. A. Butts and D. S. Rokhsar, Nature (London) **397**, 327 (1999).
[11] V. Schweikhard, I. Coddington, P. Engels, V. P. Mogendorff, and E. A. Cornell, Phys. Rev. Lett. **92**, 040404 (2004).
[12] Y. Castin and R. Dum, Eur. Phys. J. D **7**, 399 (1999).
[13] N. Papanicolaou, S. Komineas, and N. R. Cooper, Phys. Rev. A **72**, 053609 (2005).
[14] D. L. Feder, A. A. Svidzinsky, A. L. Fetter, and C. W. Clark,

Phys. Rev. Lett. **86**, 564 (2001).
[15] S. Komineas and N. Papanicolaou, Laser Phys. **14**, 571 (2004).
[16] N. N. Carlson, Physica D **98**, 183 (1996).
[17] G. H. Bauer, R. J. Donnelly, and W. F. Vinen, J. Low Temp. Phys. **98**, 47 (1995).
[18] O. K. Vorov, P. Van Isacker, M. S. Hussein, S. Yu. Kun, and K. Bartschat, AIP Conf. Proc. **777**, 72 (2005).
[19] V. Bretin, P. Rosenbusch, F. Chevy, G. V. Shlyapnikov, and J. Dalibard, Phys. Rev. Lett. **90**, 100403 (2003).
[20] N. L. Smith, W. H. Heathcote, J. M. Krueger, and C. J. Foot, Phys. Rev. Lett. **93**, 080406 (2004).